Characterization and stability of catanionic vesicles formed by pseudo-tetraalkyl surfactant mixtures

Carlotta Pucci,[a] Lourdes Pérez,[b] Camillo La Mesa,*[a] and Ramon Pons*[b]

Received (in XXX, XXX) Xth XXXXXXXXX 20XX, Accepted Xth XXXXXXXXX 20XX
DOI: 10.1039/b000000x

The phase behavior of an ad hoc synthesized surfactant, sodium 8-hexadecylsulfate (8-SHS), and of its mixtures with didecyldimethylammonium bromide (DiDAB) in water is reported. Focus is on dilute concentration regimes, at a total surfactant content < 30 mmol/kg; there vesicular aggregates may be formed. The high synergistic behavior of such catanionic mixtures is concomitant to strongly negative interaction parameters, β (≈ -18 k_BT), significant gain in the free energy of association, ΔG_{agg}, and much lower association concentration compared to the pure surfactants. Vesicles size and ζ-potential depend on the mixture composition. Hydrodynamic diameters increase by progressive addition of oppositely charged surfactant to the one in excess. Counter-intuitively, the ζ-potential becomes more negative at DiDAB molar fractions close to 0.2. The same holds in the reverse case, the ζ-potential becomes more positive after small additions of 8-SHS; anyhow, the effect is more significant in anionic-rich mixtures. This phenomenon was explained assuming a significant release of counterions and an asymmetric distribution of the two surfactants in the inner and outer vesicle leaflets. The equimolar mixtures form a cubic phase rather than the expected lamellar one. The effect of NaBr concentration on the stability of catanionic vesicles was investigated too. At high NaBr concentrations, all systems are destabilized. For DiDAB-rich vesicles flocculation is observed, while for 8-SHS-rich ones, lamellar domains are formed at the bottom of the samples. The effect played by NaBr depends on whether it is added before or after mixing the surfactants. In particular, preformed catanionic vesicles own a great kinetic stability towards addition of NaBr compared to those obtained by the other procedure.

Introduction

Mixing anionic and cationic surfactants leads to the formation of different kinds of aggregates, depending on the respective structures, overall content, mole ratios, temperature and ionic strength. The resulting mixtures, termed catanionic, show a remarkable synergistic behavior, due to the strong attractive interactions between oppositely charged species.[1,2] In particular, they aggregate at much lower values than the critical concentrations of the individual surfactants.[3]

Catanionic mixtures easily and spontaneously form vesicles by mixing the two surfactants in non-stoichiometric ratios.[4,5] These aggregates find interesting applications as model membranes, microreactors, in cosmetics[6] and drug delivery.[7-9] Compared to phospholipid-based liposomes, the preparation of catanionic vesicles does not require high energy methods (such as sonication or mechanical stresses), is simple and cheap.[10] It is possible to modulate the catanionic vesicles size and charge by changing the mole ratio between the two species;[11] this is a crucial point for preparing matrices intended for transfection technologies. In addition, the electrostatic forces play a key role in the interactions between vesicles and biomacromolecules, such as DNA and proteins.[12-15] Finally, catanionic mixtures are suitable for drug delivery because of a reduced cytotoxicity.[16] As a rule, the latter is much lower than that pertinent to the single species. A reduced cytotoxicity is presumably related to the very low concentration of the individual surfactants in the bulk.

From a practical viewpoint, it is essential to study the phase behavior of catanionic mixtures, to clarify how these systems aggregate, what kind of morphology is possible, and, finally, to determine the optimal concentrations and mole ratios at which vesicular entities are effectively formed. Vesicles stability depends on ionic strength, and it is relevant to investigate how much the addition of salts affects the stability of these systems. Therefore, the effect of added salt on vesicle properties was investigated in some detail.

In this work, we focus on aqueous catanionic mixtures composed by a cationic surfactant, didecyldimethylammonium bromide (DiDAB, not to be confused with didodecyldimethylammonium bromide, DDAB) and sodium 8-hexadecylsulfate (8-SHS), an anionic one. The latter was synthesized some time ago,[17] but its properties did not receive due attention to date.[18] From a molecular viewpoint, both species can be considered geminal surfactants. In 8-SHS the carbon atom to which the sulfate group is linked is also joined to two alkyl chains differing in length. The resulting species is, therefore, chiral. At present we do not know as to whether this fact implies

selectivity in binding towards proteins or polypeptides. In contrast to other few reports on pseudotetraalkyl catanionic mixtures, both elements of the pair contain simple polar heads. This avoids the possible influence of ionizable and polar groups as encountered with Aerosol OT or other more complex molecules.

A substantial investigation of the individual surfactants in aqueous media was performed, paying special attention to the characterization of the anionic species. The catanionic mixtures in water at different surfactants ratios and overall surfactant concentration ≤ 30 mmol/kg were investigated. Catanionic vesicles are formed in both the cationic- and the anionic-rich sides of the phase diagram. A non ancillary consequence inherent to the above behavior is the possibility for catanionic vesicles to interact electrostatically with either proteins or nucleic acids, depending on their effective charge.

Materials

Chemicals

Didecyldimethylammonium bromide (98%) was from Sigma Aldrich and used as such, after being dehydrated. Sodium 8-hexadecyl sulfate was synthesized by sulfonation of 8-hexadecanol with chlorosulfonic acid in acetic acid.[19] The resulting acid was neutralized by sodium bicarbonate. The purity of the final product was checked by ^{1}H, ^{13}C NMR and elemental analysis and is above 99%. More detailed information can be found in ESI†. Suprapur NaBr was from Merck. Water was bi-distilled using a Milli-Q four-bowl system.

Sample preparation

Solutions of the two surfactants were prepared individually by weighing appropriate amount of DiDAB or 8-SHS and diluting with water. Catanionic mixtures were formed by mixing the above solutions having exactly the same molality, at different mole ratios.

NaBr was added according to two different procedures:

1) the individual surfactant solutions were prepared in aqueous NaBr solutions at the required concentration; thereafter, the two solutions were mixed in proper ratios;
2) the salt was directly added by weight to preformed catanionic mixtures.

Methods

Light microscopy

An Olympus BX51 light microscope equipped with a Linkam TMHS 600 hot stage, controlled by a TP94 unit, was used. The microscope works in white and polarized light. Images were acquired with an Olympus C-5060 Wide Zoom digital camera.

Surface Tension

A home-made pendant drop tensiometer was employed. A surfactant solution drop is created at the end of a straight-cut Teflon tube having known internal and external diameters. The drop shape was recorded with a camera and its image corrected for spherical aberration. The background was subtracted and the resulting droplet contour fitted in a Young-Laplace equation, with a home-made golden section search algorithm. Temperature was kept at 25.0 ± 0.5 °C. The experimental surface tension values drastically change in slope at a point corresponding to the critical micelle concentration. The critical concentration, the intersection between two straight lines, is related to the excess of the surfactant at the air/water interface, Γi, according to the Gibbs absorption isotherm

$$\Gamma_i = -\left(\frac{1}{nRT}\right)\left(\frac{\partial\gamma}{\partial \ln C}\right) \quad (1)$$

There R is the universal gas constant, T the temperature, γ the surface tension, and C the concentration. The value of n is associated to the number of ions (i.e. 2 for monovalent ionic surfactants in water and 1 in presence of electrolytes in strong excess). From Γi the area per head group, A_m, was determined.

Ionic conductivity

It was measured by an Orion Cond. Cell 011010A with platinized platinum electrodes; the cell constant is 0.998 cm^{-1}. Measurements were run by a Thermo Orion 550A unit, at 25.0 ± 0.1 °C.

Potentiometric measurements

Sodium ion activity was measured by a Ross electrode connected to a high internal impedance 720Aplus Thermo Orion Multimeter.

$8\text{-}HS^-$ ion activity was measured by a home-made selective electrode. The membrane, composed by 1 wt% of an insoluble salt of the surfactant (the equimolar salt formed between 8-SHS and DiDAB), 28 wt% of poly(vinylchloride) and 71 wt% of dioctylphtalate, was placed at the end of a glass tube filled with a reference solution ($1.0 \cdot 10^{-3}$ M 8-SHS + $1.0 \cdot 10^{-3}$ M NaCl). The internal reference electrode (Saturated Calomel Electrode) was inserted in the tube. The external reference was a double junction Ross Sure Flow reference electrode with an internal solution of AgCl (Orion Nº 900002) and an external solution of 10% aqueous KNO_3 (Orion Nº 900003). Both electrodes were immersed in the solution of unknown activity and connected to a high internal impedance 720Aplus Thermo Orion Multimeter. Measurements were run at 25.0 ± 0.1 °C.

Small Angle X-ray Scattering (SAXS)

The X-ray scattering at small angles (SAXS) was performed using a S3-MICRO (Hecus X-ray systems GMBH Graz. Austria) coupled to a GENIX-Fox 3D X-ray source (Xenox, Grenoble), which produces a detector-focused X-ray beam. The Cu Kα-line radiation, with λ = 0.1542 nm, has over 97% purity and less than 0.3% Kα. The transmitted scattered radiation was detected using a PSD 50 Hecus unit working at small-angle regimes ($0.09\ nm^{-1} < q < 6\ nm^{-1}$). Temperature was controlled through a Peltier TCCS-3 Hecus unit. The samples were inserted in a flow-through glass capillary with 1.0 mm inner diameter and 20 μm wall thickness or, in case of non fluid samples, were inserted between two Mylar sheets. SAXS scattering curves were plotted as a function of the scattering vector modulus, $q = (4/\pi)\sin(\theta/2)$, where θ is the scattering angle and λ the wavelength of the incident radiation. The scattering vector was calibrated by comparison with a standard silver behenate crystalline sample (> 98% RoseChemicals Ltd.). Scattering curves were smeared by the

detector width. We used a detector-focused small beam (300 x 400 μm full width at half maximum), which widens the peaks without noticeable effect on its position. The background was subtracted from the scattering curves. The curves were scaled in absolute units by comparison with water scattering.[20,21] The instrumentally smeared experimental SAXS curves were fitted to numerical models, convoluted with beam size and detector width effects.[22] A least squares routine based on the Levenberg-Marquardt scheme was used.[23] The bilayer thickness was determined using a three-Gaussian profile based on the MCG model according to Pabst et al.[24,25]

Dynamic Light Scattering (DLS)

Measurements were run using a Malvern Zetasizer unit, Nano ZS series HT, working at λ = 638.2 nm in back-scattering mode (at 173°), at 25.0 ± 0.1 °C. A digital correlator analyzes the scattered light intensity fluctuations, $I(\mathbf{q},t)$, due to the Brownian motion of the dispersed particles, at times t and $(t + \tau)$, where τ is the delay time. The intensity autocorrelation function $G_2(\mathbf{q},t)$, was obtained according to

$$G_2(\mathbf{q},t) = \left[\frac{\langle I(\mathbf{q},t) \cdot I(\mathbf{q},t+\tau) \rangle}{\langle I(\mathbf{q}) \rangle^2} \right] = 1 + B\left|g_1(t)\right|^2 \quad (2)$$

where q is the scattering vector. $G_2(\mathbf{q},t)$ is related to the electromagnetic field autocorrelation function $g_1(\mathbf{q},t)$ through the equation

$$G_2(\mathbf{q},t) = A + B\left|g_1(\mathbf{q},t)\right|^2 \quad (3)$$

where A is the baseline and B is the intercept. The function $g_1(\mathbf{q},t)$ is expanded by a cumulant analysis,[26] where the first term provides the diffusion coefficient, D, related to the hydrodynamic radius R_H of the particles through the Stokes-Einstein equation. The second cumulant is proportional to the polydispersity index, *PdI*. Intensity distributions were obtained by analyzing the autocorrelation functions by CONTIN algorithms.[27]

ζ-potential

Electrophoretic mobility measurements, μ, were run at 25.0 ± 0.1 °C using a Laser-Doppler facility available in the DLS equipment. The dispersions were placed into U-shaped cuvettes, equipped with gold electrodes. The ζ-potential, ζ, is related to μ by the relation[28]

$$\zeta = \mu\left(\frac{4\pi\eta}{\varepsilon'}\right) \quad (4)$$

where η is the solvent viscosity and ε' is its static dielectric permittivity. In vesicular samples

Smoluchowski's approximation holds, because the electrical double layer thickness surrounding vesicles is much smaller than their radius.

Results and discussion

DiDAB characterization

The critical association values determined by conductivity and surface tension measurements are similar to literature ones.[29,30] (See Tab. 1 and Fig. S1 in ESI†). From the Gibbs isotherm (eq. 1), we obtained an area per surfactant molecule of 74 Å^2. We calculated the chain length, l, and the hydrophobic volume, V, by Tanford's formulas[31]

Table 1 CMCs, area per polar head group, A_m, and packing parameter P of DiDAB and 8-SHS, at 25.0°C.

Surfactant	CMC (mmol/kg)			A_m (Å^2/mol)	P
	Conductivity	Surface Tension	Selective Electrode		
DiDAB	1.4 ± 0.1	1.4 ± 0.15	-	74 ± 5	0.6
8-SHS	1.3 ± 0.1	2.0 ± 0.2	2.8 ± 0.3	99 ± 5	0.4

$$V = m\left(27.4 + 26.9 n_{CH_2}\right) \quad (5)$$

$$l = 1.5 + 1.265 n_{CH_2} \quad (6)$$

where sizes are in Å^2 (or Å), and m is the number of hydrophobic chains. We deduced the packing parameter, P, from the relation[31]

$$P = \left(\frac{V}{l A_m}\right) \quad (7)$$

and obtained a value of 0.6. A_m is the area per polar head group. According to the theory, P values are compatible with the existence of vesicles.[29] The observed phase sequence is: molecular solution, aggregates, and, at high surfactant concentrations, lamellar and hexagonal phases.[29, 33] The value of P increases accordingly. The phase sequence was confirmed by SAXS and polarized light microscopy (see ESI†, Fig. S2 and S3 and Tab. S1).

8-SHS characterization

The critical concentration of the above surfactant was determined by ionic conductivity, surface tension and potentiometric measurements, using a surfactant-selective electrode (see ESI†, Fig. S4). Data are summarized in Tab. 1.

From surface tension measurements the area per polar head of 8-SHS was estimated to be 99 Å^2. The corresponding packing parameter, determined by Eq.s 5, 6 and 7, is 0.4; therefore, rods or disks are the preferred geometries for 8-SHS micellar aggregates.

A crucial point to be put in evidence from data in Table 1 is that the critical thresholds for 8-SHS obtained by different methods moderately agree each other, but lie clearly out of the reproducibility limits of the different techniques. The differences observed among the reported methods could be ascribed to a not-well defined aggregation process, starting with the formation of dimers, and ending into micelles, or other entities. It is worth

noticing, on this regard, that the different techniques we used detect aggregation by measuring not strictly related parameters: this could be another reason for the occurrence of slightly different critical values. For instance, potentiometric measurements carried out by a Na^+ selective electrode (see ESI†, Fig. S4D) suggest that the aggregation process starts at a surfactant concentration close to 0.3 mmol/kg and ends at ≈ 1 mmol/kg. Above this point, counterion binding to micelles, β, is constant and close to 0.55. Therefore, aggregate formation and

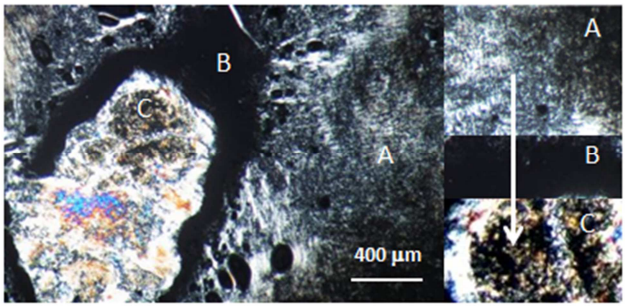

Fig. 1 Polarized light micrographs of hydrated 8-SHS in phase scanning experiments, at 25.0 °C. (A) Lamellar phase; (B) Isotropic phase; (C) fan-like textures peculiar to a hexagonal phase. The water concentration decreases from A to C, according to the direction indicated by the white arrow.

growth depends on the molecular features of the surfactant. The hypothesis of a stepwise association for 8-SHS is realistic, and has been shown to occur in surfactant with short hydrophobic chains.[34]

At 6% wt/wt in 8-SHS, giant vesicles are formed (see ESI†, Fig. S5). At higher concentrations (15, 20, and 25% wt) SAXS spectra show a broad maximum (see Supporting Information S6) with features peculiar to lipid bilayer structures.' [35,36] It is possible to identify the repetition distances from the position at 1:2 spacings; the results indicate the occurrence of lamellar order at very small q values. We evaluated the Bragg repetition distances to be 140, 115 and 85 Å for 15, 20 and 25% wt/wt, respectively. Fitting the experimental curves with a Caillé-modified analysis[24,36-38] gives a 23 Å bilayer thickness in all cases considered, while the area per molecule is 51 ± 2 $Å^2$. Since the 8-SHS hydrophobic chain in extended conformation is 11.6 Å long, no significant chain interpenetration between the two leaflets occurs. Therefore, ideal swelling occurs in the lamellar phase.

To determine the phase behavior of 8-SHS at high concentrations, phase scanning experiments by polarized optical microscopy were performed. (Fig. 1) A drop of water was placed at the outer edge of the cover-slip and allowed to diffuse into the solid. The above procedure induces a concentration gradient, and indicates a qualitative phase sequence.[39,40] At relatively high water content, a lamellar phase is met first (Fig.1A). Then an isotropic phase, presumably a cubic one (Fig. 1B), is observed. A univocal assignment on the isotropic phase structure is cumbersome. At still higher concentrations in 8-SHS it is possible to recognize fan-like textures. These are typical of a hexagonal phase, and occur at concentrations close to the hydrated crystals threshold (Fig. 1C). The observed phase is tentatively assumed to be reversed hexagonal.

Catanionic mixtures

The formation of the catanionic systems is strongly synergistic. A clear effect is the decrease of critical thresholds compared to the individual surfactants (Table 2, and ESI†, Fig. S7). The geometry of the aggregates is not easily determined *a priori*, and we prefer defining it as critical aggregation concentration, CAC rather than critical micellization, or vesiculation. The above quantity depends on mole ratios. For DiDAB-rich mixtures, the decrease in CAC values is significant, probably because this surfactant has a marked propensity to form vesicles.

Table 2 CAC, β, and ΔG_{agg} for different mole fractions in DiDAB (X_{DiDAB}), at 25.0 °C.

X_{DiDAB} (α_1)	CAC (mmol/kg)	β (k_BT)	ΔG_{agg} (kJ/mol)
0	2.0	-	-15
0.1	0.17	-11	-21.5
0.2	0.02	-18.5	-26.8
0.3	0.017	-18.7	-27.2
0.8	0.02	-18.2	-26.8
0.9	0.03	-17.8	-25.8
1	1.4	-	-15.9

From CAC values by surface tension, we estimated the interaction parameter among the two surfactants, β, at different compositions, according to[41-43]

$$\beta = \frac{\ln\left(\frac{\alpha_1 CAC_{mixt}}{X_1 CAC_1}\right)}{(1-X_1)^2} \quad (8)$$

where α_1 is the mole fraction of the 1st surfactant, CAC_{mix} is the critical aggregation concentration of the given mixture, CAC_1 that of component 1, and X_1 is the mole fraction of component 1 in the aggregate. The latter can be determined by[41]

$$\frac{(X_1)^2 \ln\left(\frac{\alpha_1 CAC_{mixt}}{X_1 CAC_1}\right)}{(1-X_1)^2 \ln\left[\frac{(1-\alpha_1) CAC_{mixt}}{(1-X_1) CAC_2}\right]} - 1 = 0 \quad (9)$$

where the meaning of each symbol is as above. The Gibbs energy of aggregation, ΔG_{agg}, was calculated according to:[44]

$$\Delta G_{agg} = RT \ln CAC \quad (10)$$

The results obtained by combining Eq. (8) and (10) are reported in Table 2.

The interactions among the components in surfactant mixtures imply negative or positive deviations from ideality of mixing. The interaction parameter, β, indicates whether positive (anti-cooperative), or negative (cooperative) contributions to the Gibbs energy take place. For all mixtures considered here β is < 0, confirming the highly synergistic behavior in the system under consideration. Its value is ≈ -18 k_BT, except when the mole

fraction of the first component is very low. When α_1 = 0.1, for instance, β is close to -11 k_BT. It is worth noticing, in addition, that β values in Table 2 are very similar to those reported in the literature for structurally related catanionic mixtures.[45]

The free energy of aggregation of catanionic systems is always more negative than the pure surfactants, indicating a substantial propensity to form mixed aggregates. Were the contributions to the Gibbs energy only ascribed to the alkyl chains, ΔG_{agg} should regularly scale with mole ratios. If additional terms are relevant,

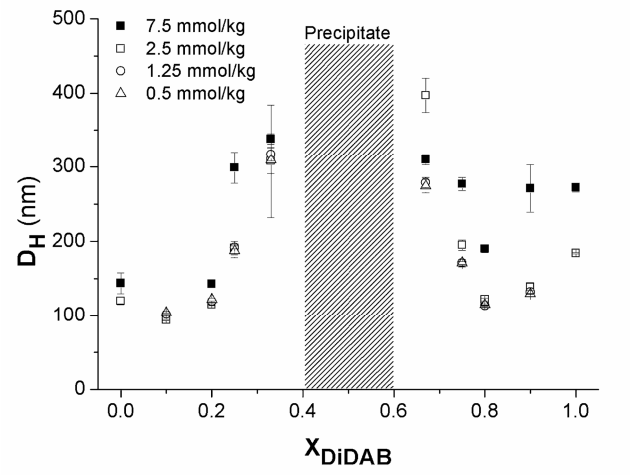

Fig. 2 The hydrodynamic diameter of vesicles, D_H (nm), as a function of DiDAB mole fraction, X_{DiDAB}, for C_{TOT} = 7.5 (■), 2.5 (□), 1.25 (○), 0.5 (Δ) mmol/kg. Measurements were run at 25.0 °C. The dashed area indicates the precipitation region.

cooperative or anti-cooperative interactions are expected to occur, as, indeed, observed. It is assumed here that the strong electrostatic interactions between oppositely charged groups facing outward the aggregate surface play a significant role in vesicle stability. A major reason is that the area per molecule in mixed systems is lower than the sum of the individual ones. That is, chains are closer and areas smaller than expected from considerations based on the behavior of the single components. In terms of the "packing constraint" theory, the interaction energy is different from that pertinent to the single systems. This hypothesis is valid in mixed mono-layers, but, very presumably, it holds in aggregate forms too.

The samples appearance depends on the mole ratio between the two surfactants. When the molar ratio of the minor component is < 0.2, for instance, the dispersions are bluish in color. This is the typical color of catanionic vesicles with sizes in the visible wavelength range.[46,47] Near equimolarity the samples are milky, and precipitates are formed. This behavior is not observed at very low mole ratios where no precipitation or bluish appearance is detected. Visual observations are confirmed by DLS measurements. (Fig. 2)

The tendency of the aggregates to change in size with mole ratios is nearly independent on the overall surfactant concentration. An abrupt increase in size is always observed close to the precipitation threshold (Fig. 2, gray area). In the DiDAB-rich region, vesicles sizes decrease up to $X_{DiDAB} \approx 0.8$ (note that 8-SHS has a lower P than DiDAB). Thereafter, aggregates with high curvature do form. Adding small amounts of 8-SHS to DiDAB dispersions reduces the aggregates curvature, leading to the formation of relatively small vesicles. This effect becomes less important when electrostatic interactions between the two surfactants occur, with subsequent increase of the average vesicles diameter.[48] The behavior in the 8-SHS-rich region is similar. In this case, however, the effect of the packing parameter goes in the contrary direction. Similar behaviour was also obtained at 15 and 30 mM.The effects on the z-potential and the size are not strictly parallel; the ζ-potential experiments will be less and less sensitive to the subtle changes as the ionic force is increased by the presence of more and more surfactant. A reasonable explanation is needed to justify the decrease of sizes in both sides of the diagram.

Because of the asymmetric composition of the vesicle inner and outer leaflets[49], the minority surfactant may concentrate preferably in one or in the other leaflets of the vesicle. Due to the geometrical constrains, the headgroups in the inner leaflet are more compacted than in the outer.[50] Because of the charge compensation and of the respective packing constrains, the minority surfactant enter the inner leaflet, with subsequent reduction in area per molecule, and lower headgroups repulsion; the process gives rise to more relaxed surface. When differences in surfactant packing become important, the formation of small vesicles is favored. Above a certain proportion, the composition of both leaflets will become similar again, inducing vesicle growth.

ζ-potential depends on the overall surfactant concentration and mole ratios, as well (Fig. 3). At high surfactant concentrations (Fig. 3A), absolute values of ζ-potentials decrease, moving towards equimolarity. This is intuitive, since oppositely charged surfactants interact electrostatically, form pseudo-tetra-chain zwitterionic species, and reduce the net charge of the aggregates. At lower surfactant concentrations, the trend is not univocal (Fig.3B). For DiDAB-rich mixtures, the ζ-potential does not change significantly upon addition of 8-SHS. In the anionic-rich side, conversely, the ζ-potential becomes more negative on increasing X_{DiDAB}. Presumably, counterion release taking place when catanionic vesicles are formed overlaps to the electrostatic interactions between DiDAB and 8-SHS. The former may dominate over ion-pair neutralization, with a net increase of vesicle surface charge density.[51] This hypothesis could explain the absence of a break point in the conductivity versus surfactant concentration plot for 8-SHS/DiDAB mixtures (data not shown). The amount of released counterions may be equivalent to that below the CAC, making cumbersome the detection of a break point.[52] In addition, as suggested by the changes in vesicular size, the proportion of minority surfactant entering the inner leaflet of the vesicles could be bigger than that in the outer leaflet and the effect is more marked when 8-SHS is added to DiDAB than in the reverse case. Therefore the electrostatic contributions in the outer leaflet are expected to be smaller for the latter case.

On this purpose, we introduce a simplified model to understand the different behavior of the two region of the phase diagram. A vesicle composed of surfactant 1 has an external radius equal to R_e. Its inner radius R_i is defined as $R_e - d$ and the radius corresponding to the center of the bilayer, R_c, is $R_e - d/2$, where d is the bilayer thickness. So, we can calculate, respectively, S_e, S_i and S_c, that is the outer, inner and central surfaces. The number of molecules that occupy these surfaces are calculated by dividing S

by the area per molecule of the surfactant 1, $A_{m,1}$. The area per molecule at the center is fixed by the minimum distance between the two methyl groups at the end of the surfactant double chain. We impose N_c to be the maximum possible number of molecules in the middle of the bilayer as a reference value. Adding one molecule of the surfactant 2 in the inner leaflet causes the transfer of one molecule of surfactant 1 in the outer leaflet and the formation of 1-2 neutral complexes. The fraction of "lost" surfactant 1 by addition of a fraction α of surfactant 2 is, therefore, 2α. The neutral complex 1-2 has a much smaller area per molecule compared to that of the individual surfactants. In addition, there are lower electrostatic and steric repulsion contributions. This implies a more relaxed situation. Supposing that S_i is not affected by the addition of the second surfactant, we may write:

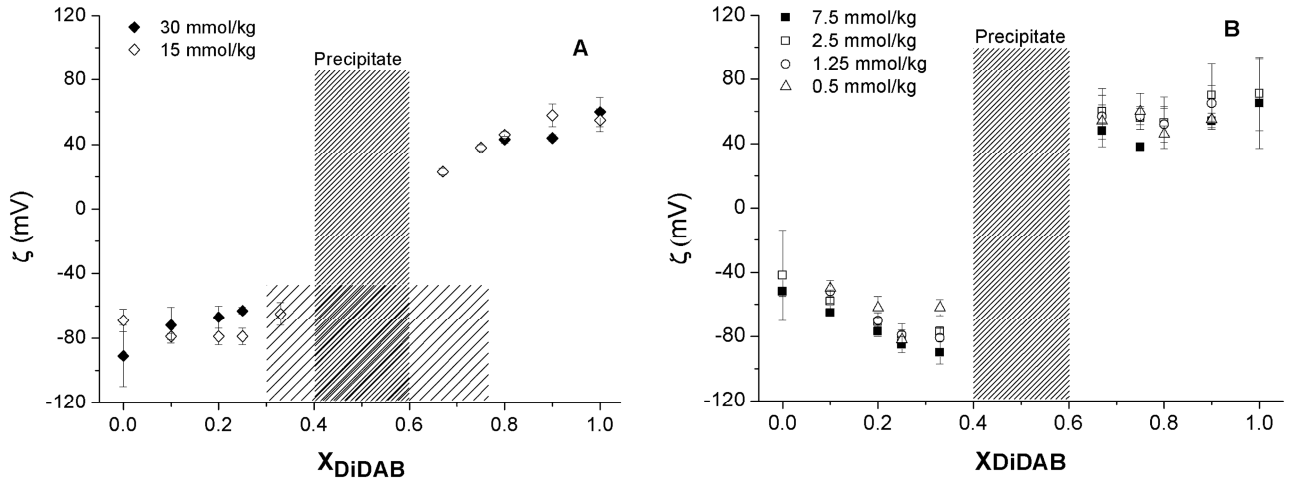

Fig. 3 ζ-potential (mV) as a function of DiDAB mole ratios, X_{DiDAB}, for surfactant concentrations, C_{TOT} = **(A)** 30 (♦) and 15 (◊) mmol/kg; **(B)** 7.5 (■), 2.5 (□), 1.25 (○), 0.5 (Δ) mmol/kg. All measurements were run at 25.0 °C. The dashed areas indicate the region where precipitation is observed. In A, the dashed area represents the precipitation thresholds for C_{TOT} = 15 mmol/kg, while the light dashed area is relative to C_{TOT} = 30 mmol/kg.

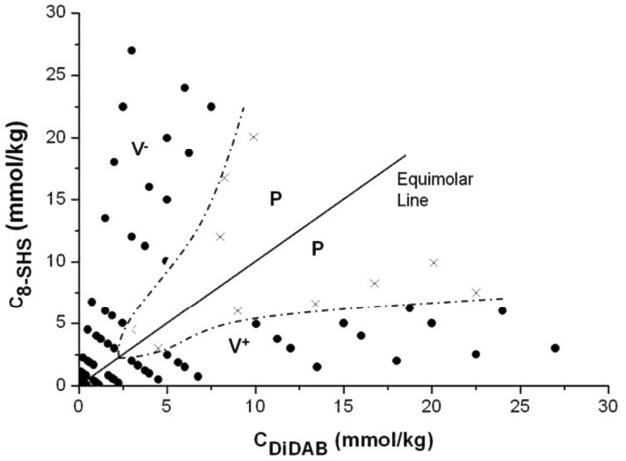

Fig. 4 Partial phase diagram of the 8-SHS/DiDAB/water system as a function of 8-SHS and DiDAB concentration, in mmol/kg, at 25°C. The equimolar line is indicated. The vesicular areas are indicated by solid circles and are denominated as V^-, in the anionic-rich and V^+ in the cationic-rich one, respectively. Points indicated by crosses are located in the precipitate area (P).

$$S_i = (N_C - 2\alpha)A_{m,1} + 2\alpha A_{m,1-2} \qquad (11)$$

where $(N_C - 2\alpha)A_{m,1}$ is the surface occupied by surfactant 1 in the inner leaflet and $2\alpha A_{m,1-2}$ is that pertinent to 1-2 complexes, with area per molecule $A_{m,1-2}$. In this way, we can calculate α, i.e. is the fraction of surfactant 2 needed to reach a relaxed inner surface, without modifying other vesicle feature, by:

$$\alpha = \frac{S_i - N_C A_{m,1}}{2(A_{m,1-2} - A_{m,1})} \qquad (12)$$

Replacing in the above equations the numerical values of each parameter, we got α in the cases of 8-SHS and DiDAB as major components, respectively. $A_{m,1-2}$ is derived from the SAXS spectrum of the precipitated 1:1 complex. Although it is a rough estimate (the complex has a cubic arrangement that could not be resolved), the value we obtained (55 Å^2) is in agreement with the trend of A_m at different X_{DiDAB} deduced from surface tension measurements. For 8-SHS α is 0.065 while for DiDAB is 0.15. Therefore DiDAB bilayer needs a larger fraction of oppositely charged surfactant to reach a relaxed inner surface. In words, the same amount of oppositely charged surfactant allows for a larger reduction of radius for the negative vesicles than for the positive ones. This agrees with the results obtained by size and ζ-potential measurements at different X_{DiDAB}.

Combining visual inspections and DLS measurements, we draw a partial phase diagram in dilute concentration regimes. In all cases considered here the mixtures are supposed to be pseudo-binary component systems (Fig. 4). Close to the equimolar line, a precipitate is formed. Contrary to what could be expected for a 1:1 precipitate of similar size molecules, its SAXS patterns do not fit in a lamellar structure (Fig. 5A). The observed peaks (having relative orders $3^{½}$, $4^{½}$, $8^{½}$) suggest the presence of a face-centered cubic arrangement (Fm3m). From the q value of the first peak, we estimated a repetition distance of 22 Å. The units forming an Fm3m arrangement are generally globular,[53,54] although at yet unknown bi-continuous structures may preserve the expected

local flat geometry. A second possibility is the presence of coexisting phases, previously observed in other catanionic mixtures.[55] In cases like such, the coexistence with lamellar phases was supposed. However, the order of the peaks does not fit in any lamellar arrangement or in others commonly reported for liquid crystalline phases. The precipitate shows strongly birefringent textures in polarized microscopy (Fig. 5B). It has been previously reported that systems with cubic symmetry may give grain colored textures, if the crystalline domains have dimensions comparable to the wavelength of light, with selective Bragg reflection. This behavior is peculiar to blue phases.[56] It is also known that such phases are liquid crystals with three-dimensional cubic defects.[57] Let us remind too that 8-SHS has a chiral carbon atom and that in condensed phases chiral selectivity may be present, producing

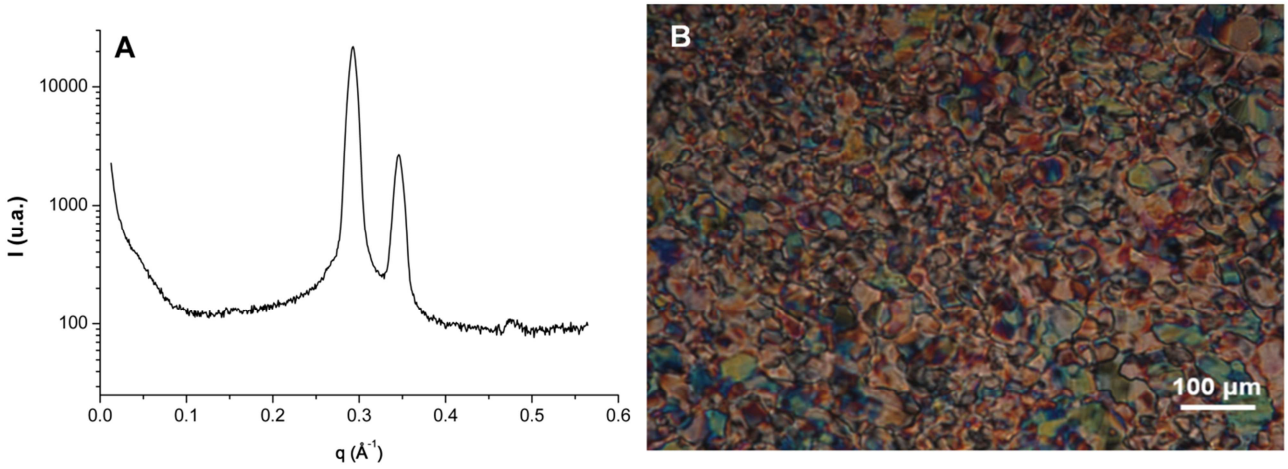

Fig. 5 SAXS curve of a dehydrated 8-SHS-DiDAB precipitate at composition close to the equimolar line and nominal surfactant concentration of 30.0 mmol/kg, at 25.0°C. **(B)** Polarized light micrograph of an 8-SHS-DiDAB precipitate at 25.0°C, having the same composition as (A).

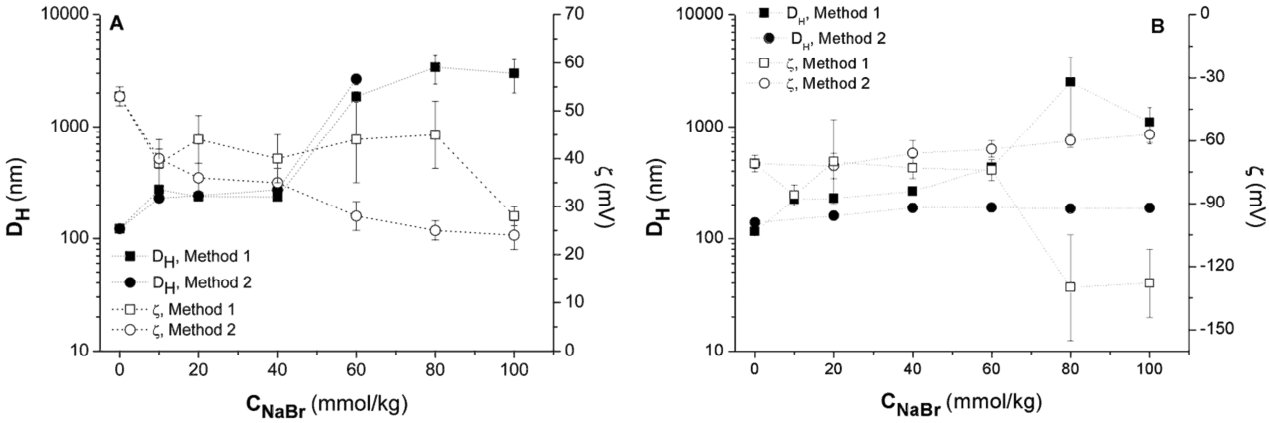

Fig. 6 (A) Hydrodynamic diameters (solid symbols) and ζ-potentials (open symbols) as a function of NaBr concentration C_{NaBr} (mmol/kg), for preparation method 1 (squares) and 2 (circles), at 25.0 °C, for positive vesicles with X_{DiDAB} = 0.8 and a total surfactant concentration of 2.5 mmol/kg **(B)** Hydrodynamic diameters (solid symbols) and ζ-potentials (open symbols) as a function of NaBr concentration C_{NaBr} (mmol/kg), for preparation method 1 (squares) and 2 (circles), at 25.0 °C, for negative vesicles with X_{DiDAB} = 0.2 and a total surfactant concentration of 2.5 mmol/kg.

Table 3 CAC of 8-SHS and DiDAB (mmol/kg) as a function of NaBr concentration, at 25.0°C. Data are deduced from surface tension (see ESI†, Fig. S8).

C_{NaBr} (mmol/kg)	$CAC_{8\text{-}SHS}$ (mmol/kg)	CAC_{DiDAB} (mmol/kg)
0	2	1.4
5	-	0.19
10	-	0.14
20	-	0.08
40	0.36	0.07
100	0.13	0.07

local enrichment in one enantiomer. This point may deserve further investigation.

Effect of salt

In view of the possible applications in biological systems it is important to know the effect of ionic strength on vesicles size and stability. To check how NaBr affects the properties of catanionic vesicles, we choose a total surfactant concentration of 2.5 mmol/kg and X_{DiDAB} equal to 0.8 for cationic-rich vesicles and 0.2 for the anionic ones.

The effect of salt on the aggregation properties of the individual surfactants was preliminarily investigated. As indicated Table 3, the CACs of DiDAB and 8-SHS are reduced in presence of NaBr. The same holds for the area per head group at the solution-aggregate interface. The effect is significant in DiDAB-based solutions. For DiDAB in 10 mmol/kg NaBr P approaches 1, and the formation of flat bilayers is favored. In presence of 40 mmol/kg of NaBr, the packing parameter P of 8-SHS becomes 0.7; in such conditions, vesicle formation is possible.

Addition of NaBr to cationic-rich vesicles (Fig. 6A) is not preparation-dependent (for further details, see the Materials section). Particles diameter increases and ζ-potential decreases

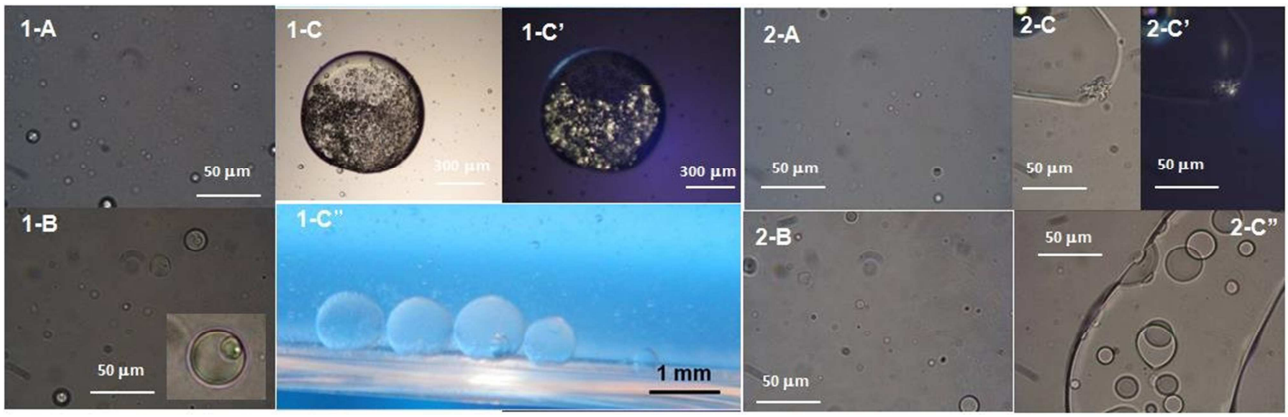

Fig. 7 (1) Optical micrographs of vesicles at X_{DiDAB} = 0.2, total surfactant concentration of 2.5 mmol/kg, C_{NaBr} = 100 mmol/kg, prepared with Method 1, at 25.0 °C: **(1-A)** after 1 day from preparation; **(1-B)** after 7 days; **(1-C)** after 20 days; **(1-C')** is **(1-C)** with polarized light; **(1-C")** Enlarged view showing the formation of droplets at the bottom of the sample 20 days after preparation. **(2)** Optical micrographs of vesicles at X_{DiDAB} = 0.2, total surfactant concentration of 2.50 mmol/kg, C_{NaBr} = 100 mmol/kg, prepared by Method 2, at 25.0 °C. **(2-A)** 1 day from preparation; **(2-B)** after 7 days; **(2-C)** and **(2-C'')** after 20 days; **(2-C')** is **(2-C)** viewed in polarized light.

with NaBr concentration. At high salt amount (above 70 mmol/kg), flocculation is observed one day from the preparation.

The situation is different in anionic-rich vesicles (Fig. 6B). Systems prepared by procedure 2 are not much influenced by addition of salt, and only small variations on ζ-potential are observed. Conversely, when NaBr is added to the surfactant solutions before mixing (procedure 1), there is an increase in sizes, when the ζ-potential become more negative. Flocculation is not observed in any case. The presence of large vesicles is confirmed by optical microscopy (Fig. 7, 1-A and 2-A), even 1 day after preparation. The systems prepared by procedure 2 do not change in 7 days; conversely, concentric vesicles are visible in samples prepared according to procedure 1 (Fig. 7, 1-B). Phase separation of droplets at the bottom of the sample is observed 20 days after preparation. The droplets are clusters of lamellar aggregates (Fig. 7, 1-C-C'-C''). In samples prepared according to protocol 2, phase separation occurs in much longer times. In 20 days, it is possible to observe cluster formation. According to Fig. 7, 2-C-C' and C" small clusters are present; In Figure 7. 2-C", in particular, it is evident that the latter are formed by the fusion or coalescence of small vesicles into big ones. In such case, phase separation is observed after a long time. Accordingly, the two preparation procedures lead to the same final state: a phase separation.

Differences detected by ζ-potential and DLS measurements can be ascribed to differences in the initial states for the two

systems and in the kinetic pathways. In method 1, NaBr is added to the individual surfactant solutions. In such conditions, CACs are low (Tab. 3) According to the packing parameter, both surfactants form lamellar entities in such conditions. It is conceivable that mixing oppositely charged lamellar dispersions does not produce the formation of mixed entities, but promotes their interaction, through electrostatic attraction. Thus, large particles aggregate, as in Fig.6B. These particles grow with time until they reach an "unstable" situation when too large. At this point phase separation occurs. In method 2, catanionic vesicles are present. They have higher kinetic stability compared to the former conditions. Therefore, addition of salt destabilizes the system more slowly. The processes involved in the two systems are nearly the same and are presumably controlled by the concentration of free surfactant ions. The only difference is the kinetics leading to the final state.

According to the DLVO theory[58], colloid stability depends on the balance between double layer repulsions and Van der Waals attraction. An increase in salt concentration destabilizes the system and promotes aggregation, fusion, coalescence, or flocculation. Procedure 1 promotes double layer repulsions between lamellar entities having the same surface charge density, and double layer attraction between those oppositely charged. Therefore, destabilization mechanisms are fast. We expect the aggregation of negatively charged vesicles onto positive ones. This situation is formally equivalent to the adsorption of a polyelectrolyte onto oppositely charged vesicles. In such case the surface charge density of the two species influences strongly their interactions.[14] Moreover, when one of the two components is in excess, the overall charge acquires the sign of the major component. The same happens when polyelectrolyte in excess is adsorbed onto vesicles.[14,59] In this way, there are strong electrostatic repulsions between particles and the system is stable.

The achievement of the final state for both procedures (1 and 2) is slow since the nucleation process leading to the formation of a lamellar phase can be long.[60] The different stability found for the cationic-rich and anionic-rich vesicles may be also due to the different absolute value of the net charge of the vesicles found in absence of salt.

Conclusions

We characterized sodium 8-hexadecylsulphate (8-SHS), an anionic double-chain surfactant. Its aggregation features slightly depend on the method of detection, indicating a complex association; a step-wise process is possible. The calculated packing parameter suggests the formation of non spherical aggregates.

Catanionic mixtures formed by 8-SHS and didecyldimethylammonium bromide (DiDAB), were investigated. CACs decrease strongly already at low surfactant mole ratios. The highly negative interaction parameter β is due to a synergistic and cooperative effect between the two surfactants. In the concentration range investigated here, vesicles are formed. Their diameter and ζ-potential depends on X_{DiDAB}. At low surfactant content, the surface charge density depends on the release of counter-ions, inducing a non trivial increase of ζ-potential values, as a result of partial charge compensation. The effect is particularly evident when 8-SHS is in excess. Vesicles size depends on X_{DiDAB}. On both sides of the equimolar line, vesicle sizes increase abruptly. However, small additions of the oppositely charged species to DiDAB, or 8-SHS, dispersions produce a reduction in diameter. This effect may be due to the asymmetric distribution of the minority surfactant in the "per se" asymmetric inner and outer vesicle leaflets. The present model predicts, in a qualitative way, that the effect should be more evident in the 8-SHS-rich side. The results agree quite well with the theory, and suggest that a non balanced composition of the inner and outer leaflets is a key parameter to take into account.

At equimolarity phase separation is observed. Surprisingly, the neutral complex has, a cubic structure, which we tentatively assign to a Fm3m symmetry. Considering also the strongly birefringent textures observed in polarized microscopy, this phase has some similarities with the well-known "blue phases". This point is very interesting and needs further investigations to be clarified.

At high NaBr concentration, the vesicular phase is thermodynamically un-favored. The destabilization occurs after a certain lapse of time, because of the high kinetic stability of the systems. Anionic-rich vesicles are more stable than cationic ones; this fact can be ascribed to the higher surface charge density of negatively charged vesicles as compared to the others.

The formation of vesicles at low surfactant content, the synergistic behavior of the mixtures, the tunability of sizes and ζ-potential, the high kinetic stability are promising in potential applications in drug delivery and non-viral gene therapy, where the features of the carriers are the key parameters to be considered.

Acknowledgments

We thank Jaume Caelles, in the SAXS-WAXS service at IQAC, for X-Ray measurements; Imma Carrera for technical assistance in the synthesis and surface tension measurements. Financial support from MINECO CTQ2013-41514-P and MAT2012-38047-CO-02 is gratefully acknowledged. Financial support from Generalitat de Catalunya 2014SGR836 is gratefully acknowledged. Financial support from "La Sapienza" University of Rome (IT) is acknowledged too.

Notes and references

[a] *Department of Chemistry, Cannizzaro Building, La Sapienza University, P.le A. Moro 5, I-00185 Rome, Italy. E-mail: camillo.lamesa@uniroma1.it*

[b] *Departament de Tecnologia Química i de Tensioactius, Institut de Química Avançada de Catalunya, IQAC-CSIC, c/ Jordi Girona 18-26, Barcelona, Spain. E-mail: ramon.pons@iqac.csic.es*

† Electronic Supplementary Information (ESI) available: Detailed synthesis procedure of 8-SHS, surface tension and conductivity measurements of the surfactants, SAXS spectra of different content water of DiDAB and 8-SHS and a summarizing table of parameters deduced by SAXS (Tab. S1); Phase scanning experiments for DiDAB; potentiometric measurements with a homemade 8-HS^- and a Na^+ selective electrodes; Surface tension measurements of the catanionic mixtures and the surfactants at different NaBr concentrations. See DOI: 10.1039/b000000x/

1 A. Khan, B. and E. F. Marques, *Current Opinion in Colloid & Interface Science*, 2000, **4**, 402-410.

2 L. M. Bergström and T. J. Bramer, *J. Colloid Interface Sci.*, 2008, **322**, 589-595.
3 K. Tsuchiya, J. Ishikake, T. S. Kim, T, Ohkubo, H. Sakai and M. Abe, *J. Colloid Interface Sci.*, 2007, **312**, 139-145.
4 E. W. Kaler, A. K. Murthy, B. E. Rodriguez and J. A. N Zasadzinski, *Science*, 1989, **245**, 1371-1374.
5 E. W. Kaler, K. L. Herrington, A. K.Murthy, and J. A. N. Zasadzinski, *J. Phys. Chem.*, 1992, **96**, 6698-6707.
6 S. Prevost and M. Gradzielski, *J. Colloid Interface Sci.*, 2009, **337**, 427-484.
7 J. H. Fendler, in *Membrane Mimetic Chemistry*. New York : John Wiley & Sons, Inc, 1982.
8 S. Bhandarkar, and A. Bose, *J. Colloid Interface Sci*., 1990, **135**, 531-538.
9 Y. Zhao, D. Zhi and S. Zhang, in *Non-Viral Gene Therapy*. ed. Y. Xu-bo, InTech, Rijeka (Croatia), 2011**,** ch. 13, pp. 293-318.
10 C. G. Ferguson, R. D. James, C. S. Bigman, D. A. Shepard, P. K. Katsambe, D. G. Myszka and G. D. Prestwich, *Bioconjugate Chem.*, 2005, **16**, 1475-1483.
11 P. Andreozzi, S. S. Funari, C. La Mesa, P. Mariani, M. G. Ortore, R. Sinibaldi and F. Spinozzi, *J. Phys. Chem. B.*, 2010, **114**, 8056-8060.
12 A. Bonincontro, C. La Mesa, C. Proietti, and G. Risuleo, *Biomacromolecules*, 2008, **8**, 1824-1829.
13 C. Letizia, P. Andreozzi, A. Scipioni, C. La Mesa, A. Bonincontro and E. Spigone, *J. Phys. Chem. B.* 2007, **111**, 898-908.
14 C. Pucci, A. Scipioni and C. La Mesa, *Soft Matter*, 2012, **8**, 9669-9675.
15 F. De Persiis, C. La Mesa and R. Pons, *Soft Matter*, 2012, **8**, 1361-1368.
16 N. Lozano, L. Perez, R. Pons and A. Pinazo, *Amino Acids*, 2011, **40**,721-729.
17 H. C. Evans, *J. Chem. Soc*., 1956, 579-586.
18 S. I. Karakashev and E. D. Manev, E. D. *J. Colloid Interface Sci.*, 2002, **248**, 477-486.
19 E. E. Dreger, G. I. Keim, G. D. Miles, L. Shedlovsky, J. Ross, *Ind. Eng. Chem.* 1944, **36**, 610-617.
20 D. Orthaber, A. Bergmann and G. Glatter, *J. App. Cryst*., 2000, **33**, 218-225.
21 L. Pérez, A. Pinazo, R. Infante and R. Pons, *J. Phys. Chem. B*, 2007, **111**, 11379-11387.
22 J. Morros, R. M. Infante and R. Pons, *Soft Matter*, 2012, **8**, 11353-11362.
23 J. S. Pedersen, *Adv.Colloid Interface Sci*,.1997, **70**, 171-210.
24 G. Pabst, G. Rappolt, H. Amenitsch and P. Laggner, *Phys. Rev. E: Stat.Phys., Plasmas, Fluids, Relat. Interdiscip. Top.*, 2000, **62**, 4000-4009.
25 G. Rodríguez, M. Cócera, L. Rubio, C. Alonso, R. Pons, C. Sandt, P. Dumas, G. López-Iglesias, A. de la Maza and O. López, *Phys. Chem. Chem. Phys.*, 2012, **14**, 14523-14533.
26 D. E. Koppel, *J. Chem. Phys.*, 1972, **57**, 4814-4820.
27 S. W. Provencher, *Comput. Phys. Commun*., 1982, **27**, 213-227.
28 A. W. Adamson, *Physical Chemistry of Surfaces.* Wiley, New York, 1990**.** ch.V, 218-226.
29 T. F. Svitova, Y. P. Smirnova, S. A. Pisarev and N. A. Berezina, *Colloids Surf. A.* 1995, **98**, 107-115.
30 P. del Burgo, E. Aicart and E. Junquera, *Colloids Surf. A.*, 2007, **292**, 165-172.
31 C. Tanford, *The Hydrophobic Effect*, J. Wiley & Sons, New York, 1980, 52.
32 J. N. Israelachvili, D. J. Mitchell and B. W. Ninham, *J. Chem. Soc. Faraday Trans. II*, 1976, **72**, 1525-1568.
33 G. G. Warr, R. Sen, D. F. Evans and J. E. Trend, *J. Phys. Chem.*, 1988, **92**, 774-783.
34 M. Collinet-Fressancourt, L. Leclercq, P. Bauduin, J. M. Aubry and V. Nardello-Rataj, *J. Phys. Chem. B*, 2011, **115**, 11619-11630.
35 J. Bolze, T. Fujisawa, T. Nagao, K. Norisada, H. Saido and A. Naito, *Chem. Phys. Lett.*, 2000, **329**, 215–220.
36 E. Haba, A. Pinazo, R. Pons, L. Pérez and A. Manresa, *Biochimica et Biophysica Acta – Biomembranes*, 2014, **1838**, 776–783.
37 R. Zhang, R. M. Suter and J. F. Nagle, *Phys. Rev. E*, 1994, **50**, 5047-5060.
38 R. Zhang, S. Tristram-Nagle, W. Sun, R. L. Headrick, T. C. Irving, R. M. Suter and J. F. Nagle, *Biophys. J.*, 1996, **70**, 349-357.
39 A. S. C. Lawrence, *Mol. Cryst. Liq. Cryst.*, 1969, **7**, 1−57.
40 M. Figueira-Gonzalez, V. Francisco, L. Garcia-Rio, E. F. Marques, M. Parajo and P. Rodriguez-Dafonte, *J. Phys. Chem. B*, 2013, **117**, 2926-2937.
41 P. Mukerjee and A. Yang, *J. Phys. Chem*., 1976, **89**, 1388-1390.
42 P. C. Schulz, J. L. Rodriguez, R. M. Minardi, M. B. Sierra and M. A. Morini, *J. Colloid Interface Sci*., 2006, **303**, 264-271.
43 M. J. Rosen, *Surfactants and Interfacial Phenomena*, Wiley-Interscience, New York, 2004, 3rd ed., ch. 11, 380-381.
44 D. F. Evans and H. Wennestrom, *The Colloidal Domain: Where Physics, Chemistry and Biology Meet*, Wiley-VHC, New York, 1994, ch. 4, 142.
45 R. Muzzalupo, G. Gente, C. La Mesa, E. Caponetti, D. Chillura-Martino, L. Pedone and M. L. Saladino, *Langmuir*, 2006, **22**, 6001-6009.
46 E. I. Franses, L. E. Scriven, W.G. Miller and H. T. Davis, *J. Am. Oil Chem. Soc*., 1983, **60**, 1029-1042.
47 E. I. Franses, L. E. Scriven, W.G. Miller and H. T. Davis, *J. Am. Oil Chem. Soc*., 1983, **60**, 1043-1049.
48 E. F. Marques, O. Regev, A. Khan, M. Miguel and B. Lindman, *J. Phys. Chem. B*, 1999, **103**, 8353-8363.
49 H. T. Jung, B. Coldren, J. A. Zasadzinski, D. J. Iampietro and E. W. Kaler, *PNAS*, 2001, **98**, 1353-1357.
50 P. K. Yuet and D. Blankschtein, D. *Langmuir*, 1996, **12**, 3802-2818.
51 N. Lozano, A. Pinazo, C. La Mesa, L. Pérez, P. Andreozzi and R. Pons, R. *J. Phys. Chem. B.*, 2009, **113**, 6321-6327.
52 K. Tsubone, Y. Arakawa and M. J. Rosen, M. J. *J. Colloid Interface Sci*., 2003, **262**, 516-524.
53 S. S. Soni, G. Brotons, M. Bellour, T. Narayanan and A. Gibaud, *J. Phys. Chem. B*, 2006, **110**, 15157-15165.
54 M. Mandal and M. Kruk, *J. Phys. Chem. C*, 2010, **114**, 20091–20099.
55 B. F. B. Silva, E. F. Marques, U. Olsson and R. Pons, *Langmuir*, 2010, **26**, 3058–3066.
56 H. Kikuchi, M. Yokota, Y. Hisakado, H. Yang and T. Kajiyama, *Nature Materials*, 2002, **1**, 64-68.
57 H. J. Coles, and M. N. Pivnenko, *Nature*, 2005, **436**, 997-1000.
58 D. F. Evans and H. Wennerstrom, *The Colloidal Domain: where Physics, Chemistry, Biology and Technology meet*, Wiley-VHC, New York, *1994*, Ch. 8.1-8.2, 330-335.
59 C. Pucci, A. Salvia, M. G. Ortore and C. La Mesa, *Soft Matter*, 2013, **9**, 9000-9007.
60 L. L. Brasher, K. L. Herrington, E. W. Kaler, *Langmuir*, 1995, **11**, 4267-4277.

Supporting Information

Characterization and stability of catanionic vesicles formed by pseudotetraalkyl mixtures

Carlotta Pucci[1], Lourdes Pérez[2], Camillo La Mesa[1*], Ramon Pons[2*]

1. Department of Chemistry, Cannizzaro Building, La Sapienza University, P.le A. Moro 5, I-00185 Rome, Italy

2. Departament de Tecnologia Química i de Tensioactius, Institut de Química Avançada de Catalunya, IQAC-CSIC, c/ Jordi Girona 18-26, Barcelona, Spain.

Preparation of 8 sodium hexadecyl sulfate

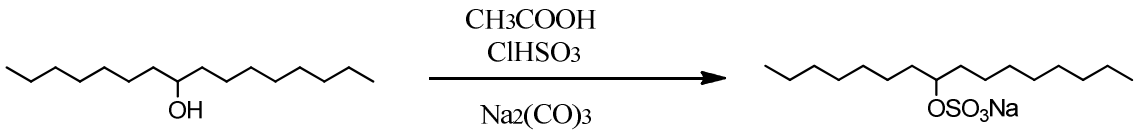

To 2 mL of acetic acid 0.66 mL (10x 10^{-3} mols) of chlorosulfonic acid were added at 0-5 ºC with stirring. Then 2 gr (8.2 x 10^{-3} mols) of 8-hexadecanol were added drop wise and the mixture was stirred during 30 minutes at 4 ºC. After that the reaction mixture was poured on 30 grams of cracked ice and 30 mL of n-butanol were added. The end of the reaction was checked by TLC using as eluent a mixture of ciclohexane/ isopropyl ether/acetic acid (86:14:0.8). Finally the solution was neutralized using sodium carbonate and then sufficient solid sodium bicarbonate was added in order to keep the solution saturated with inorganic sodium salts. The target compound was separated with the butanol layer and the aqueous layer was further extracted four times with butanol. The butanol extract was concentrated under vacuum to remove the water and the inorganic salts were separated by filtration. The butanol was removed under vacuum and the solid obtained was crystalized in methanol/acetonitrile.

Analytical data and spectral assignments:

Yield: 78%, **MW**: 344.2 g.mol^{-1}, **ESI-MS**, m/z= 321 corresponding to $(M+H)^+$. **Elem. Analy.** Found: C, 54.3; H, 9.6; S, 8.8; Cal. for $C_{16}H_{33}NaO_4S$-0.5H_2O, C, 54.3; H,9.8; S, 9.0.

^{1}HNMR: δ_H (CD_3OD), 0.8 [t, 6H, -C<u>H</u>$_3$, alkyl chain], 1.2-1.4 [m, 24H, -C<u>H</u>$_2$-, alkyl chain], 1.6 [m, 4H, -C<u>H</u>$_2$-CH(SO_4Na)-C<u>H</u>$_2$-], 4.4 [m, 1H -C<u>H</u>(OSO_3Na)-]. **^{13}CNMR:** δ_H (CD_3OD), 14.4 [<u>C</u>H_3-, alkyl chain], 23.7, 26.1, 30.4, 30.6, 30.7, 30.8, 33.0, [-<u>C</u>H_2-, alkyl chain], 35.2 [-C<u>H</u>$_2$-CH(SO_4Na)-C<u>H</u>$_2$-], 80.9 [-C<u>H</u>(SO_4Na)-].

Methods

The structure of the pure compound was checked by ^{1}H and ^{13}C nuclear magnetic resonance (NMR) analyses which were recorded on a Varian spectrometer at 499.803(^{1}H) and 125.233 (^{13}C) MHz, respectively, using the deuterium signal of the solvent as the lock. Chemical shifts (δ) are reported in parts per million (ppm) downfield from tetramethylsilane (TMS). All measurements were carried out on 0.6 mL samples in 5 mm tubes using a 5 mm indirect broadband probe. ^{13}C NMR spectra were recorded under composite decoupling to eliminate ^{13}C-^{1}H coupling.

Mass spectroscopy (MS) spectra with fast atom bombardment (FAB) or electrospray techniques were carried out with a VG-QUATTRO from Fisons Instruments. Elemental analysis of the final compounds was also achieved.

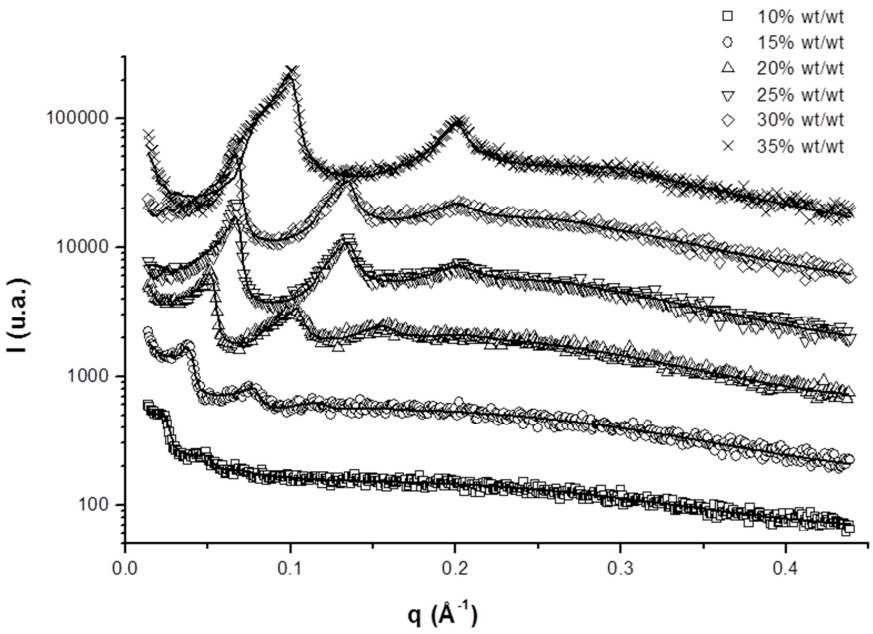

Figure S1. SAXS spectra of DiDAB solutions at 10.0 (squares), 15.0 (circles), 20.0 (up triangles), 25 (down triangles), 30.0 (rhombuses) and 35.0 wt/wt% (cross) in water, at 25.0°C. The solid lines represent the fits obtained by a modified Caillè analysis.

% wt/wt	d (Å)	A_m (Å^2/mol)
35	63.0	61
30	76.0	59
25	96.8	56
20	122.9	55
15	167.6	54
10	285.5	49

Table S1. Bragg repetition distances and area per surfactant molecule derived from SAXS spectra of DiDAB solutions in water at different wt/wt% at 25.0 ºC.

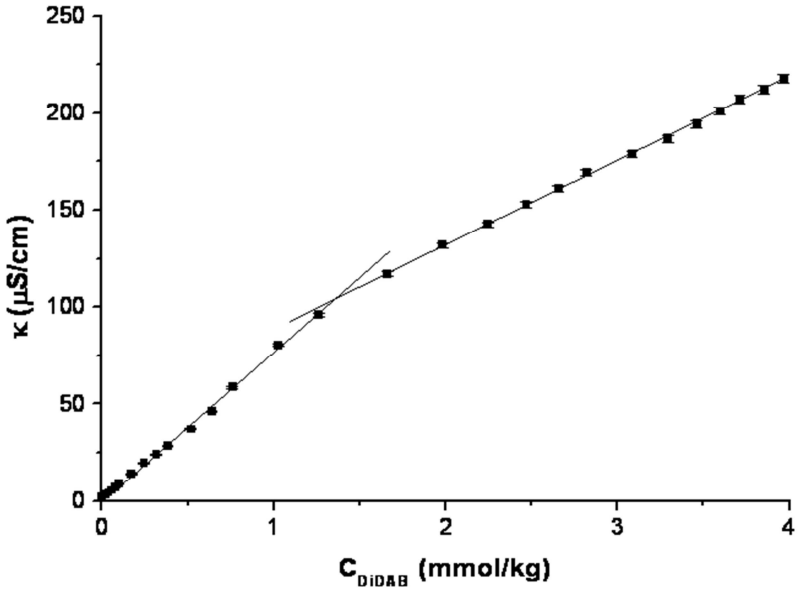

Figure S2. Conductivity, κ, (μS/cm) vs DiDAB concentration (mmol/kg) at 25.0 ºC. The intersection of the straight lines identified the CMC.

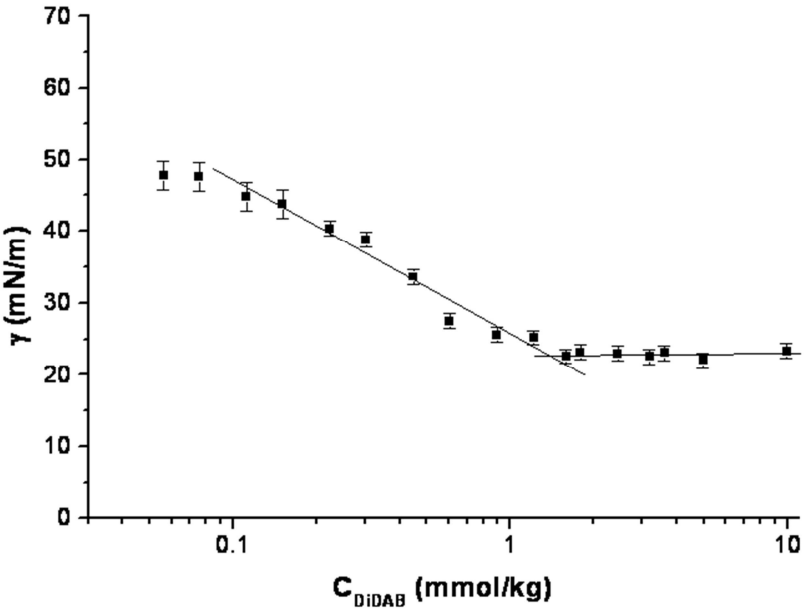

Figure S3. Surface tension, γ, (mN/m) vs DiDAB concentration (mmol/kg) at 25.0 ºC. The intersection of the straight lines identified the CMC.

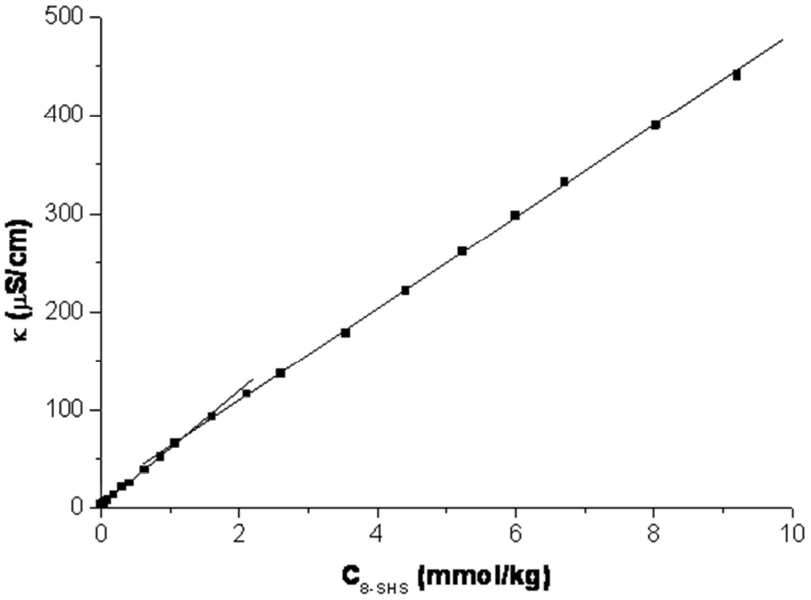

Figure S4. Conductivity, κ, (μS/cm) vs 8-SHS concentration (mmol/kg) at 25.0 ºC. The intersection of the straight lines identified the CMC.

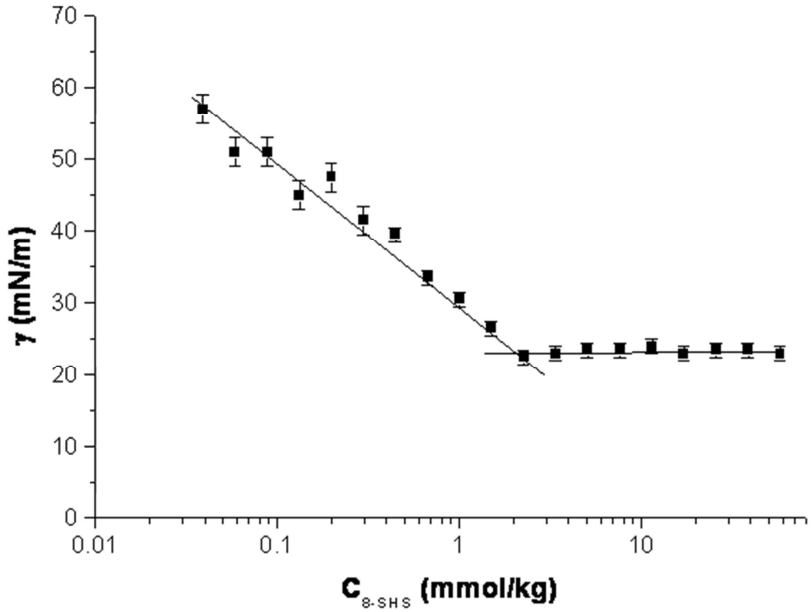

Figure S5. Surface tension, γ, (mN/m) vs 8-SHS concentration (mmol/kg) at 25.0 ºC. The intersection of the straight lines identified the CMC.

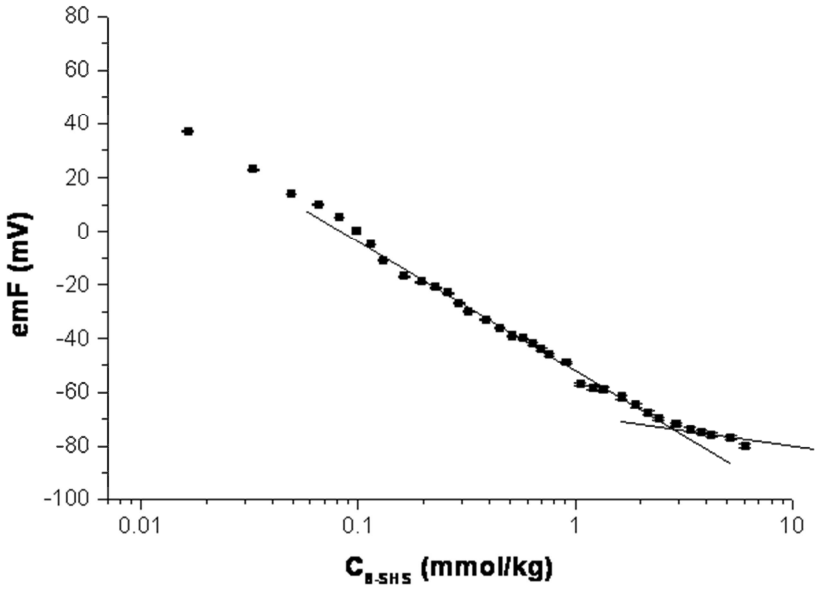

Figure S6. Electromotive force, emF, (mV) vs 8-SHS concentration (mmol/kg) at 25.0 ºC. The intersection of the straight lines identified the CMC.